communications earth & environment

Article

A Nature Portfolio journal

Article in Press

https://doi.org/10.1038/s43247-026-04118-2

Chlorophyll extremes during a surface marine heatwave in a seasonally stratified shelf sea

Check for updates

Charlotte A. J. Williams [1] ✉, Beth E. Scott [2], Tom P. Rippeth [3], Zoe L. Jacobs[4], Juliane U. Wihsgott [5], Matthew R. Palmer[6], Rory O'Hara Murray [7] & Joanne E. Hopkins[4]

Marine heatwaves are increasing in frequency and intensity globally against a background of long-term climate warming, yet their impacts on subsurface biogeochemistry in temperate shelf seas remain poorly constrained. Here, we present high-resolution in situ observations of chlorophyll during a Category IV marine heatwave in June 2023, collected using an autonomous ocean glider in a seasonally stratified shelf sea. Surface chlorophyll exhibited a rapid but short-lived enhancement, increasing from <1 mg m^{-3} to >5 mg m^{-3} and briefly exceeding the climatological ±2σ range by up to 40%. In contrast, subsurface chlorophyll showed a sustained enhancement, with concentrations within the subsurface chlorophyll maximum increasing from typical post-bloom values of 1–2 mg m^{-3} to >3 mg m^{-3} and episodic peaks exceeding 9 mg m^{-3}. This intensification was accompanied by an increase in depth-integrated chlorophyll, reaching 140 mg m^{-2}. Accelerated bottom mixed-layer warming and strengthened horizontal temperature gradients are consistent with a possible influence of horizontal transport processes, while elevated surface irradiance may also have contributed. These findings highlight the importance of sustained, vertically resolved observations for detecting ecosystem responses to climate extremes.

Marine heatwaves (MHWs), a term describing high ocean temperature events, can have profound ecological, economic, and societal consequences[1,2]. MHWs have been shown to have significant impacts on marine ecosystems, leading to shifts in community compositions and species migration[3], as well as mass mortality and biodiversity loss with economic consequences[1,4]. One example of catastrophic MHW impacts was the 2014–2016 MHW in the northeastern Pacific, which caused significant declines in salmon and sardine populations and led to economic losses for coastal communities, as well as mass seabird mortality[5].

Recent studies have indicated that MHWs have become longer-lasting and more frequent, extensive and intense in the past few decades, largely as a consequence of long-term ocean warming, with these trends predicted to accelerate under continued climate change[6–9]. The year 2023 witnessed record-breaking MHWs across the globe[10], which resulted in coral bleaching and mortality, as well as ocean circulation changes[11]. In the North Atlantic, a recent study demonstrated that the 2023 MHWs were exacerbated by shallow mixed layers, which are set to continue in the future[12,13].

There is a growing interest in ocean biogeochemical extremes that can co-occur with MHWs[7,14]. Chlorophyll-*a* concentration is widely used as a proxy for phytoplankton biomass, as it represents the primary photosynthetic pigment common to phytoplankton, although the relationship between chlorophyll and carbon biomass can vary with community composition and physiological state[15,16]. Phytoplankton provides the base of the marine food web, and MHW-low chlorophyll extremes have been associated with low fish biomass conditions[17].

Stratification is an important control on light and nutrient availability for marine phytoplankton[18,19]. During MHWs, increased surface temperatures can strengthen near-surface stratification[20], potentially reducing nutrient supply to the euphotic zone and affecting phytoplankton growth[18,21]. However, MHWs are not driven solely by local surface heating; horizontal advection can also contribute to their development through the transport of anomalously warm water masses[22,23], which may also contain different nutrient properties. On continental shelves, the influence of open-ocean mesoscale eddies is often limited by the shelf break, but cross-shelf

[1]National Oceanography Centre, Liverpool, UK. [2]School of Biological Sciences, University of Aberdeen, Aberdeen, Scotland, UK. [3]School of Ocean Sciences, Bangor University, Anglesey, Wales, UK. [4]National Oceanography Centre, Southampton, UK. [5]Plymouth Marine Laboratory, Plymouth, UK. [6]School of Biological and Marine Sciences, University of Plymouth, Plymouth, UK. [7]Scottish Government Marine Directorate, Marine Laboratory, Aberdeen, Scotland, UK.
✉e-mail: chwill@noc.ac.uk

exchanges and the advection of different water masses can nevertheless modify local nutrient distributions and phytoplankton growth conditions.

Furthermore, MHWs may cause a 'shoaling' of the surface mixed layer (SML), also known as a 'shallow MHW'[14], reducing the depth to which wind-driven mixing penetrates and concentrate phytoplankton production into a shallower region of the water column. This process alters both light availability and may influence nutrient supply pathways. In addition, ocean temperature extremes are known to influence phytoplankton physiology, affecting cellular growth and respiration rates[24,25]. The magnitude and direction of these responses depend on environmental context, including latitude, phytoplankton community composition, and the relative importance of light and nutrient limitation.

The impact of MHWs on phytoplankton varies regionally. In nutrient-limited low- and mid-latitude regions, enhanced stratification during MHWs often reduces nutrient supply to the euphotic zone, leading to declines in surface chlorophyll[7,26–28]. In contrast, MHWs can increase chlorophyll in light-limited environments by alleviating temperature and light constraints on growth[1,29,30]. Consequently, phytoplankton responses depend strongly on the balance between nutrient and light limitation[30].

Temperate shelf seas exhibit a distinct seasonal cycle. During spring, the onset of seasonal stratification and development of a thermocline facilitate the spring bloom by retaining phytoplankton in the nutrient replete euphotic zone. As the bloom progresses nutrients become depleted in surface waters, and the thermocline acts as a barrier separating the warm, nutrient-depleted surface layer from cooler, nutrient-rich deeper waters. A subsurface chlorophyll maximum (SCM) typically forms at the thermocline and the base of the euphotic zone, where sufficient light and nutrient supply coexist[18], supported by intermittent nutrient fluxes from the bottom mixed layer (BML) across the thermocline[18,31–33]. The SCM can persist throughout summer and contribute substantially to total phytoplankton biomass, primary production and carbon cycling in stratified shelf seas[34]. Despite its ecological importance, the response of SCMs to MHWs remains poorly understood because most observations of chlorophyll variability are derived from satellite ocean-colour products that are limited to near-surface waters. Consistent with this, a recent study found no statistically significant relationship between MHWs and surface chlorophyll anomalies around the UK[7], although satellite observations cannot resolve subsurface structure where much of the phytoplankton biomass may reside during summer[18,34].

Record breaking MHWs occurred globally in 2023[10]. A category IV MHW (extreme) is classified by NOAA as when sea surface temperatures (SSTs) were greater than their average by four times their daily 90th centile deviation[35]. In June 2023 a category IV MHW occurred around the UK, one of the most intense events recorded in UK waters, with SSTs exceeding +5 °C above the climatological average for June in some regions[7,36,37]. Here we show the impact of this extreme warming event on subsurface chlorophyll in a temperate, seasonally stratified shelf sea, using high-resolution results from an autonomous vehicle deployed during the MHW. We hypothesise that the MHW had an impact on both the surface and subsurface chlorophyll concentrations.

Results

June 2023 Marine heatwave

Average monthly SST anomalies for UK waters showed a clear progressive warming relative to the 30-year climatology during April–June 2023 (Fig. 1b–d). From April to June 2023, SST anomalies around UK waters evolved from weak, fairly uniform warming of up to 1 °C to a strong, widespread MHW in June with SST anomalies exceeding 5 °C in some regions, including our study site (Fig. 2a). In April, anomalies were moderate (up to +1 °C) and spatially consistent across UK waters. By May, warming intensified but became more uneven, with stronger positive SST anomalies in the western and southern shelf areas and relatively cooler conditions in some parts of the northern North Sea, however, our study site still showed a monthly average SST anomalies of up to +1 °C. By June, intense warming was evident across almost all regions, with our study site in the northwestern North Sea emerging as a clear local hotspot, playing host to an average SST anomaly of >+3 °C over the month of June.

The full daily 2023 SST time series from our study site, relative to the 30-year climatology, showed that SSTs exceeded the climatological 90th percentile from the beginning of the year (Fig. 2a). Satellite-derived SST showed excellent agreement with in situ glider measurements collected during the deployment period (Supplementary Fig. 4a; $R = 0.99$, RMSE = 0.51 °C, $N = 107$), providing confidence that the satellite and reanalysis products accurately captured the timing and magnitude of the June 2023 warming event. A two-week Category I MHW occurred from 1 January despite wintertime, typically fully mixed conditions, indicating that anomalous surface temperatures were not confined to stratified summer periods but persisted intermittently throughout the year. A further three short-lived (< 1 week) Category I MHWs developed prior to spring (March). Immediately before the glider deployment commenced on 1 May, an additional Category I MHW occurred in mid-April, spanning 13–21 April. During the glider deployment, an intense and rapidly escalating MHW in June 2023 occurred. The MHW began on 2 June as a Category I MHW, intensified to Category II by 9 June, and reached Category III by 13 June, before peaking at Category IV (SST > 16 °C) on 16 June. SSTs remained in Category IV for approximately one week before gradually declining, although conditions continued to meet MHW thresholds until 30 June. This resulted in a month-long MHW event, representing the most severe MHW recorded in this region over the 30-year observational record (Supplementary Fig. 5).

Surface chlorophyll during the MHW

Over the wider UK, positive and negative monthly surface chlorophyll anomalies were present throughout June 2023. In our study region, chlorophyll anomalies were positive on average during June relative to the climatology (Fig. 3a). However, these patterns were derived from monthly averages of surface chlorophyll and therefore do not resolve the short-term variability, including daily fluctuations in chlorophyll associated with the evolving MHW. Analysis of the daily 2023 surface chlorophyll time series from our study site revealed more variability relative to the monthly climatology (Fig. 2b). Surface chlorophyll generally remained within the ±2σ bounds for most of the year and increased on 11 June, during the intensification phase of the MHW from <1 mg m^{-3} to 2–3 mg m^{-3} (Fig. 2b), peaking at >5 mg m^{-3} on 14 June according to the satellite ocean colour data. This was the largest deviation from the climatological range observed for 2023, coinciding with the peak of the MHW when SST was greatest (Fig. 2a). This spike in surface chlorophyll concentrations was also evident in the glider observations (Figs. 2b and 4d). Comparison of satellite-derived and in situ glider surface chlorophyll measurements showed a statistically significant positive relationship ($R = 0.65$, $p = 1.8 \times 10^{-13}$; Supplementary Fig. 4b), indicating that both datasets captured the same broad temporal variability in surface chlorophyll during the deployment. However, the glider observations resolve higher-frequency variability and capture short-term spikes in surface chlorophyll that are less apparent in the satellite record. This discrepancy arises because satellite products represent daily composites at relatively coarse spatial resolution, whereas glider measurements provide high-resolution in situ surface observations at 2–3 h timescales and point locations. Consequently, short-lived or spatially heterogeneous features may be smoothed or underrepresented in the satellite data.

The June 2023 surface chlorophyll peak (> 5 mg m^{-3}) lay above the climatological ±2σ upper bound (3–4 mg m^{-3}), marking an anomalously high event and an exceedance of up to 40% above the typical June upper envelope.

Subsurface glider observations during the MHW

While SST clearly showed the onset and intensification of the June MHW, the glider observations demonstrated that this warming was associated with the development of strong stratification (Fig. 4b, c). During the period of enhanced SML warming, near-surface temperatures exceeded 17 °C, while

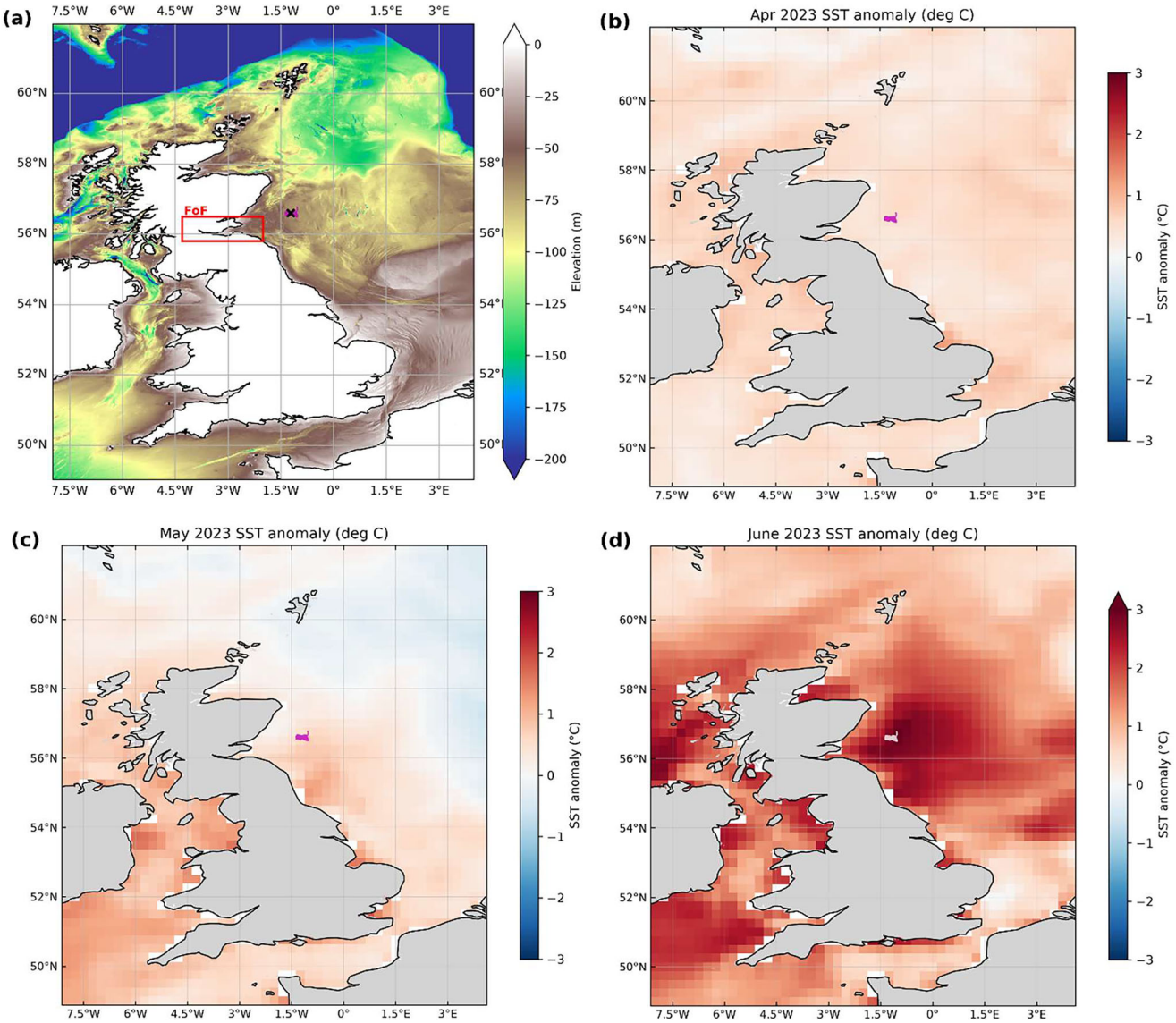


Fig. 1 | a Bathymetry of the northwestern North Sea study region showing the glider sampling track (magenta line). The Firth of Forth (FoF) is outlined by the red box; the glider survey was conducted offshore and east of this region. The black cross marks the location (56.6°N, 1.25°W) from which Earth observation variables, including sea surface temperature (SST) and surface chlorophyll concentration, were extracted. **b**–**d** Monthly SST anomalies relative to the 1992–2022 climatology from ERA5 for **b** April, **c** May, and **d** June 2023. The glider track is shown in magenta in (**b**) and (**c**), and in white in (**d**) for improved visibility against the stronger positive SST anomalies. Positive anomalies indicate warmer-than-average monthly sea surface temperatures, with the strongest warming occurring in June during the marine heatwave.

cooler waters (8–9 °C) persisted in the BML, resulting in a pronounced thermocline separating the SML and BML. The SML progressively shoaled during the onset of the MHW, reaching a minimum depth of 3.4 m on 13 June and remaining close to this minimum for more than five days (until 18 June). This prolonged period of a shallow SML coincided with the most intense phase of surface warming and the development of strong vertical density gradients (Fig. 4c), indicative of highly stratified conditions.

In temperate shelf seas, the BML, located beneath the seasonal thermocline, gradually warms throughout the stratified period due to diapycnal (vertical) transfer of heat from the surface into deeper waters. BML temperature at our study site increased steadily throughout the glider sampling period (Fig. 4b), with the warming rate increasing from 0.014 °C day^{-1} between 8 May and 1 June to 0.019 °C day^{-1} during the marine heatwave period (1–30 June; Supplementary Fig. 6). This represents a 33% increase in the rate of BML warming. Comparison of the fitted trends showed that the increase was highly significant ($z = 17.84$, $p < 0.001$). The timing of this enhanced warming coincided with the onset of the MHW, indicating that heat reached deeper waters during the event.

In stratified shelf seas, vertical exchange across the seasonal thermocline is generally facilitated by turbulent diapycnal mixing, which transports heat and other tracers between surface and deeper waters[38–42]. In temperate shelf seas, nutrient-rich waters are typically located below the thermocline; consequently, enhanced mixing across this interface would increase the upward flux of nutrients into the nutrient-limited euphotic zone[18,31–33,41] and here. However, the June 2023 MHW was associated with enhanced stratification and a pronounced shoaling of the surface mixed layer (Fig. 4c), conditions that would generally be expected to suppress turbulent diapycnal exchange across the thermocline. To assess the potential role of horizontal advection in BML warming, a simple back-of-the-envelope calculation was performed using along-track BML temperature gradients derived from the glider observations. Median absolute horizontal temperature gradients within the BML increased from approximately 0.004 °C km^{-1} prior to the

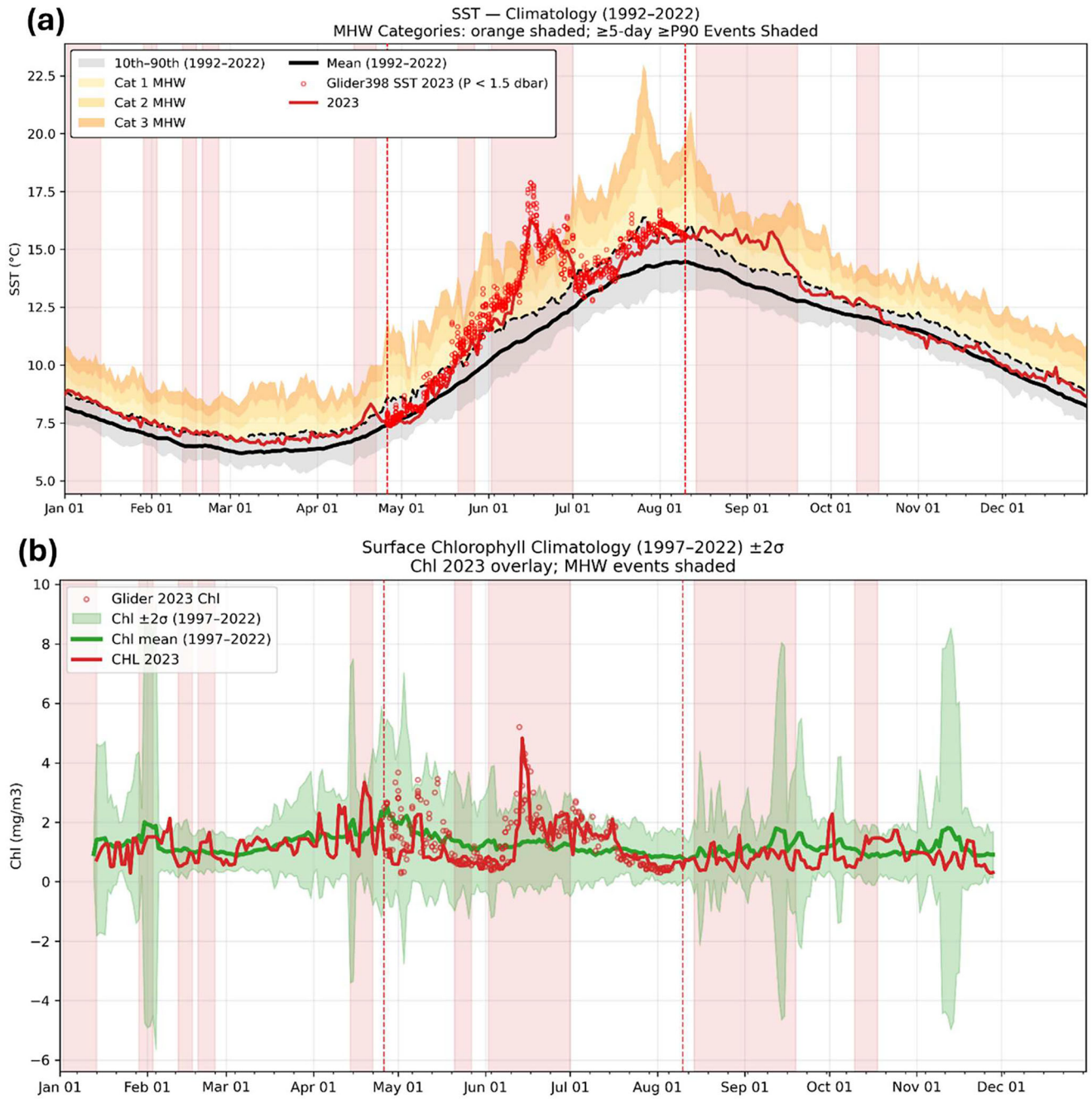


Fig. 2 | a Glider-location sea surface temperature (SST) from ERA5 for 2023 (red line), shown alongside in situ glider SST measurements (red open circles) and the 1992–2022 climatology (thick black line). The 10th–90th percentile range of the climatology is shown by the grey shading, with the 90th percentile threshold indicated by the black dashed line. Marine heatwave (MHW) categories following Hobday et al. (2018) are shown in shades of orange; the upper boundary of the Category III shading marks the threshold for Category IV MHW conditions. Red shaded regions indicate MHW events in 2023, defined as periods of at least 5 consecutive days exceeding the 90th percentile climatological threshold. Vertical dashed red lines denote the glider sampling period. **b** Surface chlorophyll-*a* concentration from the Copernicus GlobColour Bio-Geo-Chemical L4 daily satellite product, showing the 1997–2022 climatology (green line), ±2 standard deviations (green shading), the 2023 chlorophyll record (red line), and in situ glider chlorophyll measurements (red open circles). Red shaded regions indicate MHW events as defined in (**a**).

MHW to 0.008 °C km^{-1} during the event, indicating enhanced lateral temperature gradients during the MHW. Assuming a representative residual current velocity of 0.1 m s^{-1}, horizontal temperature gradients of only ~0.0005 °C km^{-1} would be required to generate the observed increase in BML warming (0.005 °C day^{-1}). The observed gradients were therefore approximately an order of magnitude larger than this threshold, suggesting that horizontal advection potentially could have contributed to the observed enhanced BML warming.

The upper boundary of the BML exhibited persistent vertical oscillations throughout the observation period (Fig. 4b–e). The signal had a characteristic period of approximately 12–13 h, suggesting modulation by semidiurnal tidal (M_2 period = 12.42 h) and internal-wave processes. These motions periodically displaced the BML boundary by several metres, resulting in substantial variability in the thickness of the stratified interior layer. Spatial variability along the glider trajectory may also have contributed to the observed fluctuations, as horizontal gradients in thermocline depth

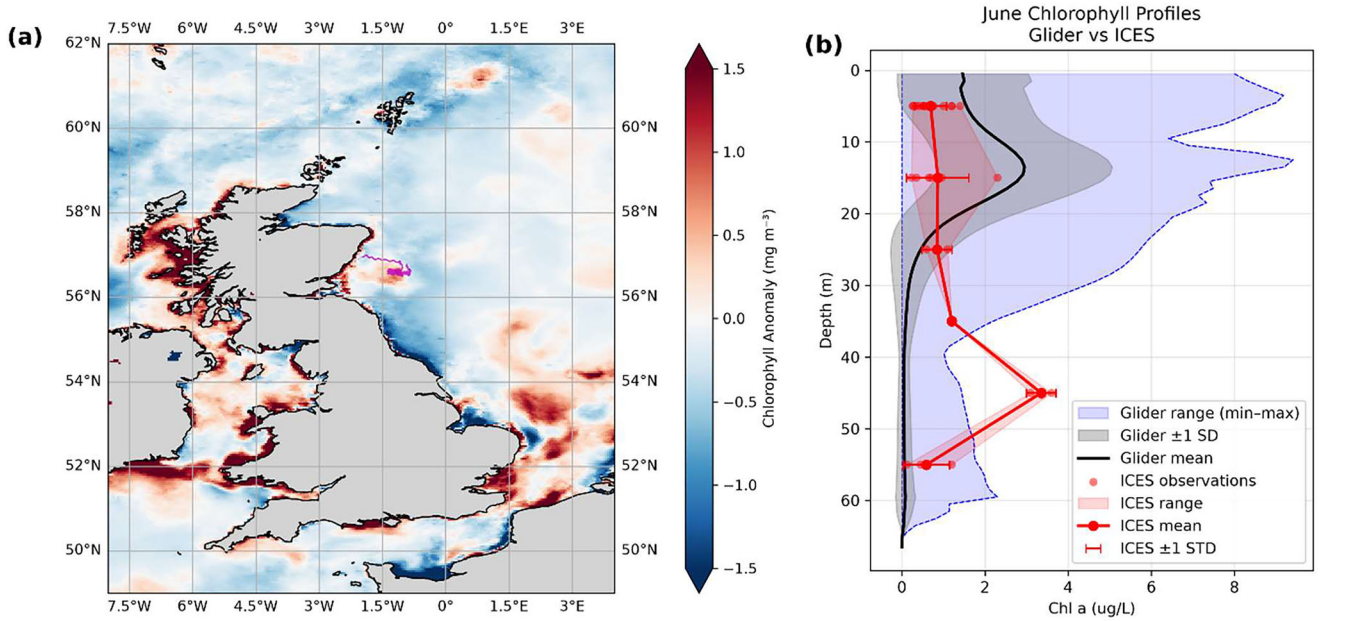


Fig. 3 | a Monthly chlorophyll-*a* anomalies for June 2023 across the wider UK shelf region derived from ocean-colour observations obtained from the Copernicus Climate Data Store (Version 6). The glider sampling track within the northwestern North Sea study region is shown by the magenta line. **b** Historical June chlorophyll profiles from the study region derived from discrete ICES observations shown alongside autonomous glider measurements during the June 2023 marine heatwave. Individual ICES chlorophyll observations from discrete water samples are shown as red points and grouped into 10 m depth intervals. The red line indicates the depth-binned mean chlorophyll concentration, horizontal error bars show ±1 standard deviation, and the red shading indicates the full range of ICES observations within each depth bin. The black line shows the mean chlorophyll profile measured by the glider throughout June 2023. Grey shading indicates ±1 standard deviation of the glider observations and blue shading indicates the full range (minimum to maximum) of glider-observed chlorophyll concentrations.

and stratification can be aliased into apparent temporal variability in the glider time series.

As expected for this time of year, phytoplankton were nutrient-limited in the SML following the spring bloom, as evidenced by inorganic nutrient profiles collected in early May, prior to the onset of the MHW (Supplementary Fig. 7). These profiles show depleted nitrate throughout the water column, with lower concentrations in the surface waters (0.54 μM) compared to the BML (0.96 μM). This represents an approximate difference of 0.42 μM, with nitrate concentrations in the BML 78% higher than at the surface (Supplementary Fig. 7). Glider observations also indicate low surface chlorophyll concentrations before the MHW (0.5–1 mg m^{-3}; Fig. 4d). However, depth-integrated chlorophyll (0–65 m) was elevated in early May (between 80 and 100 mg m^{-2}; Fig. 5b), suggesting that chlorophyll from the earlier spring bloom had been mixed throughout the water column prior to the onset of sustained stratification and the glider sampling period.

Prior to the MHW, chlorophyll concentrations within the SCM (1–2 mg m^{-3}) were typical of the post-bloom period following surface nutrient depletion. Following the onset of the MHW, SCM chlorophyll concentrations increased to ~3 mg m^{-3} and remained elevated between 11 and 18 June (Fig. 4d). During this period, the SCM experienced episodic chlorophyll peaks that frequently exceeded 3 mg m^{-3} and occasionally reached >9 mg m^{-3}.

This chlorophyll enhancement was accompanied by increased optical backscatter within the surface layer and SCM (Fig. 4e), consistent with an increase in suspended particle concentrations and/or particle size. The absence of a persistent increase in backscatter within the BML suggests that the signal was largely biological in origin rather than the result of sediment resuspension.

Consistent with these depth-resolved observations, depth-integrated chlorophyll (0–65 m) increased following the onset of the MHW and peaked on 17 June at 120–140 mg m^{-2} (Fig. 5b). The simultaneous increase in SCM chlorophyll concentrations and depth-integrated chlorophyll indicates an increase in total water column chlorophyll inventory, rather than a simple vertical redistribution of existing chlorophyll within the water column. The SCM enhancement was also outside of the climatological range. Historical ICES observations show that maximum June chlorophyll concentrations rarely exceed 3 mg m^{-3} (Fig. 3b), whereas the glider recorded multiple short-lived events exceeding this threshold and reaching >9 mg m^{-3}. Although mean SCM concentrations during the MHW remained broadly consistent with climatological values, the high-frequency glider observations revealed transient extremes that are absent from the historical record.

Following the peak of the MHW, SCM chlorophyll, depth-integrated chlorophyll and optical backscatter all returned toward pre-event levels (Figs. 4d, e and 5b). The discrepancy between the glider and historical observations likely reflects the limited temporal resolution of traditional sampling programmes, suggesting that short-lived subsurface chlorophyll extremes may be systematically underrepresented in climatological datasets.

Discussion

The year 2023 experienced record-breaking MHWs, with the North Atlantic witnessing the longest recorded MHW in the region[10]. This study examines subsurface chlorophyll enhancement during a marine heatwave on the North-western European shelf. Using high-resolution observations from an autonomous ocean glider we resolve the vertical structure of temperature, density, and chlorophyll within UK shelf seas during the MHW event in June 2023. This MHW event was driven by anomalous atmospheric conditions[12,36], a shoaling of the SML and ocean preconditioning[12,13]. Through this dataset we were able to offer insights into how MHWs may influence temperate shelf sea ecosystems.

The June MHW rapidly intensified, reaching Category IV conditions in mid-June, and was associated with strong surface warming and pronounced stratification. The SML shoaled to <3.4 m on 13 June, while temperature differences of ~8–9 °C developed across the thermocline. This resulted in a clear decoupling between the surface and subsurface layers. Surface chlorophyll exhibited a rapid but short-lived response, increasing from <1 mg m^{-3} to >5 mg m^{-3} and briefly exceeding the climatological range. However, this surface signal persisted for less than two days, suggesting that

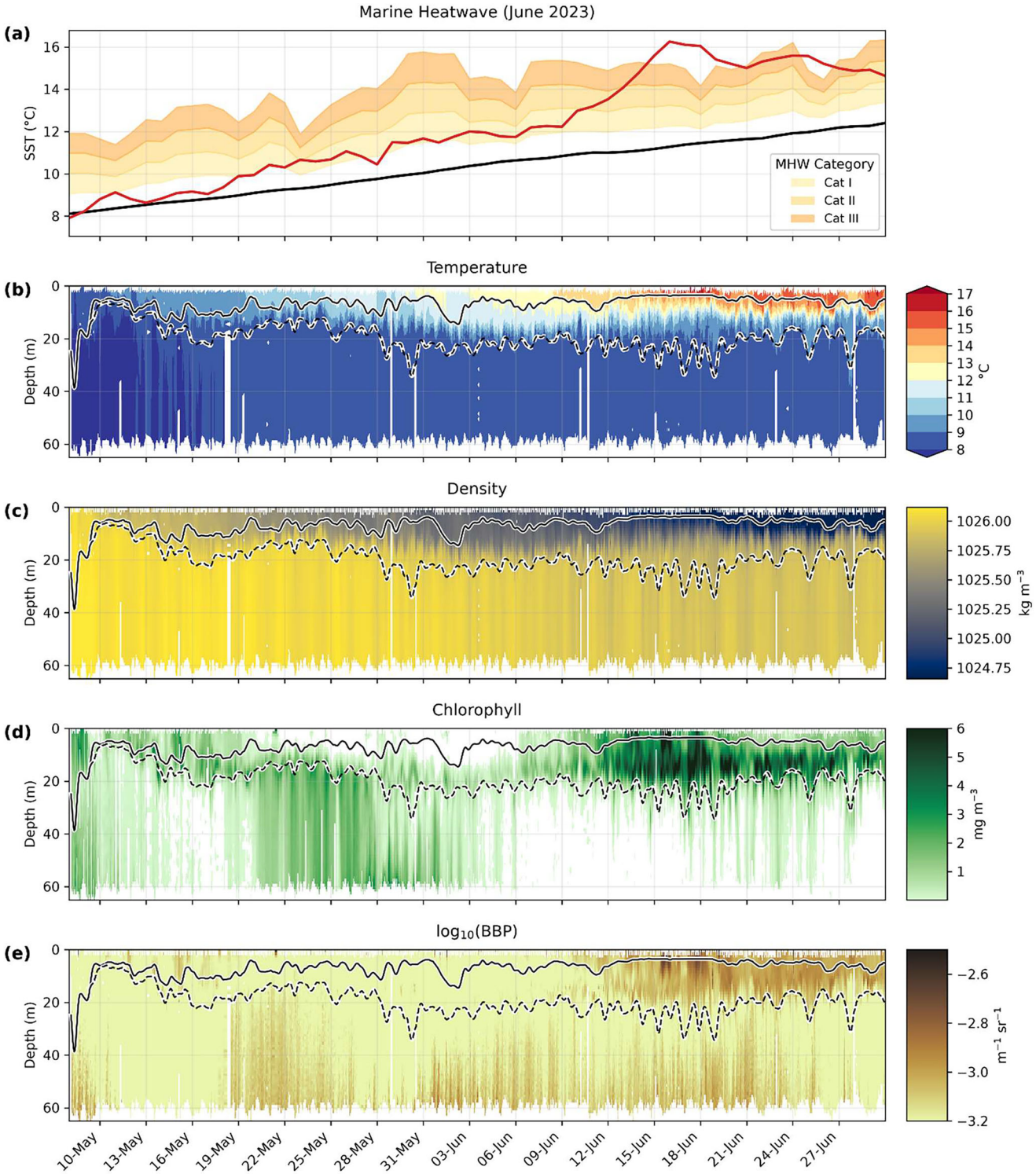


Fig. 4 | Glider transect showing **a** sea surface temperature (SST, °C) with identified marine heatwave (MHW) categories and SST anomalies relative to climatology, **b** temperature (°C), **c** potential density (kg m^{-3}), **d** chlorophyll-*a* concentration (mg m^{-3}), and **e** uncalibrated particulate backscatter (BBP; m^{-1} sr^{-1}). Solid and dashed solid black lines indicate the surface mixed layer (SML) and bottom mixed layer (BML) boundaries, respectively, determined using the de Boyer Montégut mixed-layer depth criterion. The uncalibrated BBP is displayed on a logarithmic (log_{10}) scale to enhance the visibility of regions of elevated particle backscattering. High-frequency variability at the thermocline reflects vertical movement associated with tides and internal waves, together with spatial variability in thermocline depth sampled by the moving glider and aliased into the time series.

surface observations alone provide only a partial and transient view of ecosystem responses during MHWs.

In contrast, subsurface observations reveal a more sustained response. Chlorophyll concentrations within the SCM increased significantly following the onset of the MHW, with values rising from typical post-bloom levels of 1–2 mg m^{-3} to >3 mg m^{-3} and episodically exceeding 9 mg m^{-3}. These peaks exceed the historical June range derived from ICES observations, which rarely surpass 3 mg m^{-3}, indicating that the event represents a

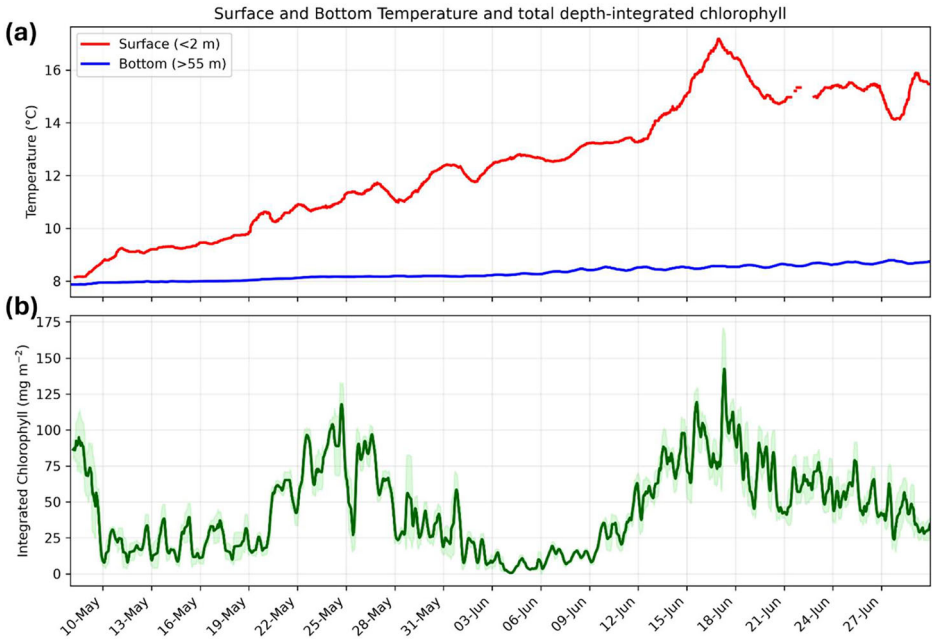


Fig. 5 | a Surface (< 2 m; red) and bottom (> 55 m; blue) temperature (°C) time series derived from the glider observations. **b** Water-column-integrated chlorophyll (0–65 m; mg m^{-2}) calculated from glider chlorophyll profiles. The dark green line shows the smoothed depth-integrated chlorophyll time series, while the light green shading indicates ±1 standard deviation based on the temporal variability of the observations.

substantial deviation from climatological conditions. Importantly, this enhancement was accompanied by a concurrent increase in total water column depth-integrated chlorophyll, which peaked at 140 mg m^{-2} during the peak phase of the MHW. The increase in integrated chlorophyll indicates that this response reflects a genuine increase in the total water column chlorophyll inventory.

Increases in observed chlorophyll concentration may occur through several mechanisms, including enhanced cellular chlorophyll content through photoacclimation[43] or increased phytoplankton biomass resulting from cell growth and division. Variability in water-column structure can also alter chlorophyll concentrations through the vertical redistribution of existing biomass. Shoaling of a phytoplankton-rich layer can increase local chlorophyll concentrations without a corresponding increase in total biomass. However, the combination of elevated chlorophyll concentrations within the SCM and increased depth-integrated chlorophyll observed here indicates that the response reflected an increase in total water-column chlorophyll inventory. Furthermore, optical backscatter, used as a proxy for particle concentration, increased during the MHW, particularly within the SML and SCM. The absence of an increase in the BML suggests that the observed particle enhancement was not driven by sediment resuspension but instead reflects an increase in biological material. The observed subsurface response is also consistent with emerging evidence that MHW-driven subsurface chlorophyll increases are particularly pronounced at temperate-high latitudes, where stratified conditions coincide with strong seasonal nutrient gradients[44].

The observations presented here do not allow us to definitively distinguish the drivers of the elevated chlorophyll concentrations during the MHW, but they do demonstrate that subsurface chlorophyll exceeded climatological norms during the event. The observed acceleration in BML warming during the MHW indicates enhanced heat transport to deeper waters in the study region. A simple order-of-magnitude assessment suggests that horizontal advection may have contributed to this warming, as median along-track BML temperature gradients increased from approximately 0.004 °C km^{-1} prior to the MHW to 0.008 °C km^{-1} during the event, indicating a strengthening of horizontal temperature gradients. These gradients were sufficiently large that plausible residual currents could generate temperature tendencies comparable to the observed increase in BML warming. Consequently, the enhanced BML warming may reflect horizontal advection of warmer water masses during the MHW that cannot be resolved from the available observations.

The enhancement of subsurface chlorophyll may have resulted from changes in nutrient supply, changes in light availability, or a combination of both. Enhanced nutrient supply could have occurred through either diapycnal mixing or horizontal transport of water masses with different biogeochemical characteristics. The observed increase in BML warming and strengthening of horizontal temperature gradients is consistent with a potential influence of horizontal advection on subsurface water properties during the event. Such transport may have altered nutrient availability if advected water masses possessed different biogeochemical characteristics. In contrast, the enhanced stratification associated with the MHW would generally be expected to suppress diapycnal mixing across the thermocline[14]. Horizontal advection is increasingly recognised as an important contributor to the development and evolution of subsurface marine heatwaves, particularly where warming is associated with the horizontal displacement of temperature gradients and fronts or the advection of warmer water masses[45]. Similarly, large-scale circulation and warm-water advection have been shown to influence the subsurface structure and depth extent of marine heatwaves, with advection-driven events extending substantially deeper into the water column than marine heatwaves driven primarily by surface air-sea heat fluxes[46].

Changes in the light environment may also have contributed to the observed chlorophyll response. In high-latitude regions, MHW-induced shoaling of the surface mixed layer has been shown to increase light exposure and alleviate light limitation, enhancing phytoplankton growth in both surface and subsurface waters[28,29]. Surface irradiance was elevated during the June 2023 MHW (Supplementary Fig. 8), consistent with the reduced cloud cover reported for the wider north-west European event[36]. However, the extent to which this increase in surface irradiance enhanced light availability at the depth of the SCM cannot be determined. Light availability below the surface depends on attenuation within the water column, which varies with chlorophyll concentration and other particles. Direct measurements of water column photosynthetically active radiation, turbulent dissipation, nutrients, and horizontal currents were not available, preventing a quantitative assessment of the relative importance of these mechanisms. Additionally, it is also important to consider that changes in phytoplankton community composition may contribute to the observed chlorophyll variability. Previous studies have shown that MHWs can drive shifts from diatom- to dinoflagellate-dominated communities[47], resulting in a cascading effect on higher trophic levels, including commercial fish stock and

seabirds. While species composition cannot be resolved in this study, such shifts may play a role and represent an important avenue for future work.

These findings highlight a critical limitation of satellite-derived ocean colour products. Surface observations alone cannot distinguish between increased biomass and physical concentration due to mixed layer shoaling, nor can they resolve subsurface dynamics such as the SCM, which often supports a large fraction of post-bloom primary production[34]. The decoupling observed here between surface and subsurface chlorophyll responses demonstrates the importance of vertically resolved observations for accurately assessing ecosystem responses to extreme events.

From an ecological perspective, the timing, magnitude and composition of a potential phytoplankton response to MHWs may have major implications for higher trophic levels, including direct effects on zooplankton grazers and fish larvae[48–52]. Phytoplankton cell size influences carbon flow in the ocean, small cells mainly recycle carbon within the microbial food web, while large cells are more likely to be grazed directly by larger zooplankton including fish larvae[48,51]. Furthermore, greater downward export of particulate organic carbon is made by large phytoplankton cells[53–55]. Additionally, increased phytoplankton biomass may also impact dissolved oxygen concentrations later in the stratified period following the microbial respiration of sinking organic detritus below the thermocline.

In conclusion, this study demonstrates that an extreme Category IV marine heatwave was associated with elevated subsurface chlorophyll concentrations in a temperate shelf sea. While surface chlorophyll exhibited only a brief enhancement, the SCM displayed prolonged increases in chlorophyll concentration and depth-integrated chlorophyll inventory that exceeded historical June observations. The mechanisms responsible for this response could not be resolved from the available observations but may involve changes in light availability (due to reduced cloud cover), differences in nutrient supply and recycling (remineralisation), potentially altering nutrient bioavailability, enhanced horizontal transport of water masses with different biogeochemical characteristics, or a combination of these processes. More broadly, the results here demonstrate the value of autonomous gliders for capturing ecosystem responses that would be largely missed by surface observations alone and highlight the need for adaptive, vertically resolved observing systems capable of resolving rapid biogeochemical change during future climate extremes.

Methods

Satellite observations of SST

SST climatologies and anomalies were derived from the ERA5 reanalysis dataset, obtained from the Copernicus Climate Data Store. ERA5 provides hourly global fields of SST at 0.25° spatial resolution, from which daily means were calculated. For UK-wide analyses, monthly mean SST fields were computed for the period 1993–2022 to generate a 30-year climatology and used to calculate monthly SST anomalies for April–June 2023. For the study site, a 30-year daily climatology (1993–2022) was constructed from the hourly ERA5 data by first computing daily mean SST, then calculating the climatological mean and associated 10th and 90th percentiles for each day of the year. The 2023 daily SST time series at the study site was compared against this climatology to identify exceedances of the 90th percentile.

MHWs at the study site were identified from the daily SST time series following the definition of Hobday et al.[35]. A MHW event was defined as a period of at least five consecutive days during which SST exceeded the seasonally varying 90th percentile of the 30-year climatology. The intensity of each event was classified relative to the difference between the climatological mean and the 90th percentile threshold, such that Category I (moderate) events occur when SST exceeds the threshold, Category II (strong) when anomalies exceed twice this difference, Category III (severe) when three times this difference is exceeded, and Category IV (extreme) when anomalies exceed four times this threshold. In this study, a fixed 30-year baseline climatology (1993–2022) was used to identify and classify MHWs, rather than a time-varying baseline that accounts for long-term ocean warming. Consequently, the identified MHWs in this study include the influence of the climate warming trend. While there is emerging evidence on the use of fixed and detrended baselines for MHW detection[56], the fixed baseline approach adopted here follows the current Hobday et al. standard for MHW detection and enables consistent comparison with previous studies.

Climatologies and anomalies of surface and subsurface chlorophyll

To investigate how surface and subsurface chlorophyll concentrations during the June 2023 MHW compared to typical conditions, climatologies were constructed from historical observations. Daily surface chlorophyll climatologies (1997–2022) were derived from ocean colour data obtained via the Copernicus Climate Change Service (C3S) Ocean Colour Version 6 dataset, which provides global daily merged satellite chlorophyll-*a* products from SeaWiFS, MERIS, MODIS Aqua, VIIRS, and OLCI[57]. From this climatology, the daily mean surface chlorophyll and associated variability (± 2 standard deviations) were calculated to define the expected range of typical conditions. The June monthly climatology (1993–2022) derived from this satellite ocean colour dataset was also used to compute June 2023 chlorophyll anomalies across a broader UK shelf region.

To characterise typical subsurface chlorophyll structure, a June climatology was constructed using historical in situ quality-controlled observations from the ICES (International Council for Exploration of the Sea) database. All available discrete chlorophyll measurements within the study region (Supplementary Fig. 1) for the month of June were extracted and combined without restriction on year to maximise sampling coverage (years 2007 to 2024, $n = 29$). Profiles were interpolated onto a common depth grid, after which depth-resolved statistics were calculated. At each depth, the mean chlorophyll concentration, standard deviation, and full range (minimum to maximum) were derived to quantify the expected vertical distribution and associated variability. This framework allowed anomalies in 2023 observations to be assessed relative to the historical mean and full observed range of variability.

Glider measurements

A shallow-water-rated, buoyancy driven Teledyne Webb Slocum glider was deployed on the Scottish shelf in the northwestern North Sea, east of the Firth of Forth, region on 26 April 2023 from the M.V. Temora operated by Marine Scotland as part of the ECOWind funded PELAgIO project (Fig. 1a). The glider was equipped with a Seabird SBE42 GPCTD sensor to measure temperature, salinity and pressure and a Seabird WETLabs ECO Puck Triplet to measure chlorophyll *a* fluorescence, backscatter (700 nm) and coloured dissolved organic matter (CDOM, not shown here). The glider was operated and piloted by MARS (Marine Autonomous Robotic Systems at the National Oceanography Centre, Southampton) to maintain repetitions of a 16 km long E-W transect between two waypoints (56.617 N, 1.375 W and 56.642 N, 1.117 W) until 10 August 2023, when it was recovered by the MPV Minna (Marine Scotland). The glider collected measurements within 10 m of the seabed and 5 m of the surface on most dives, with each dive taking approximately 20 min. Each leg of the transect took <1 day to complete. This study focuses on observations collected between 8 May and 30 June 2023, capturing conditions before the onset of the June 2023 MHW and throughout its duration.

Glider conductivity was corrected for thermal inertia[58], and nearby (< 1 km) CTD measurements collected by the RV Corystes (5–10 May 2023) were used to calibrate the derived glider salinity. Seawater density was subsequently calculated. Glider fluorescence was corrected for Non-photochemical quenching (NPQ), which suppresses fluorescence under high light conditions. NPQ was corrected using the glidertools optics package following Thomalla et al.[59] prior to any chlorophyll calibration. This approach uses the relationship between fluorescence and optical backscatter to estimate quenching effects by referencing nighttime profiles and applying a depth-dependent correction to daytime data. The quenching depth is determined from differences between daytime and nighttime fluorescence profiles, and a correction factor is derived from the fluorescence-to-backscatter ratio. Comparison of raw and NPQ-corrected fluorescence

profiles showed consistent vertical structure and SCM characteristics, indicating that the observed SCM was not an artefact of quenching (Supplementary Fig. 2). We note that the fluorescence–chlorophyll relationship may vary with phytoplankton community composition and physiological state. The calibration used here is based on bottle samples collected during May and therefore represents an empirical relationship appropriate for the study region at that time. Potential temporal variability in this relationship, particularly during the June MHW, introduces uncertainty in absolute chlorophyll concentrations; however, the primary analysis focuses on relative changes in chlorophyll structure and magnitude, which are robust to these uncertainties.

Discrete water samples analysed for chlorophyll-*a* concentration and fluorescence measurements from a ship-mounted CTD were used to calibrate the glider fluorometer to units of chlorophyll (mg m^{-3}) (Supplementary Fig. 3). Calibration was performed by matching glider observations in density space with calibrated CTD chlorophyll fluorescence profiles using strict temporal and spatial constraints (within 1 km and 30 min), in order to minimise mismatch associated with vertical displacement of water masses and fine-scale variability in the thermocline and peaks in subsurface chlorophyll. A linear regression was applied to relate glider fluorescence to extracted chlorophyll concentrations (SI.2, $n = 100$, $R^2 = 0.948$, $p = 7.13 \times 10^{-65}$, $y = 1.45x - 1.53$). An unconstrained regression (i.e. allowing a non-zero intercept) was used, as no independent dark count or blank measurement was available for the glider fluorometer. The resulting regression accounts for residual baseline fluorescence arising from electronic dark current and optical background offsets in the glider.

Definition of water-column layers

In order to characterise changes in the vertical structure of the water column during the MHW, the SML and BML boundaries were identified from individual glider density profiles. The SML depth was calculated from individual glider density profiles using a density threshold criterion. A reference density was obtained at 3 m depth, and the SML was defined as the shallowest depth at which density exceeded the reference value by 0.05 kg m^{-3}, following the methodology of de Boyer Montégut et al.[60]. A 3 m reference depth was selected to minimise the influence of near-surface variability while retaining sensitivity to changes in upper-ocean stratification. The upper vertical extent of the BML was estimated using a density-threshold approach referenced to the density at the deepest measurement. For each density profile, the deepest valid density measurement was used as the reference value, and the upper boundary of the BML was defined as the shallowest depth from the seabed at which density differed from the bottom density by more than 0.05 kg m^{-3}. This approach identifies the transition between the well-mixed near-bed layer and the stratified interior water column. For the purposes of this study, the thermocline is defined as the stratified region between the surface mixed layer (SML) and the bottom mixed layer (BML), separating the well-mixed surface and bottom layers.

To reduce the influence of short data gaps and high-frequency variability, the resulting SML and BML depth time series were smoothed using a one-dimensional Gaussian filter prior to plotting. The smoothed SML and BML boundaries were used to characterise temporal changes in stratification during the marine heatwave.

Data availability

The glider dataset is available through the British Oceanographic Data Centre and is cited under: Williams C.A.J.; Scott B. (2026). Slocum glider delayed mode data from units 306 and 398 in the Firth of Forth between April and August 2023. NERC EDS British Oceanographic Data Centre NOC. https://doi.org/10.5285/4c2fe1b0-c140-b645-e063-7086abc0c54f10.5285/4c2fe1b0-c140-b645-e063-7086abc0c54f.

Received: 28 August 2025; Accepted: 22 September 2026;
Published online: 08 October 2026

References

1. Smale, D. A. et al. Marine heatwaves threaten global biodiversity and the provision of ecosystem services. *Nat. Clim. Chang.* **9**, 306–312 https://doi.org/10.1038/s41558-019-0412-1 (2019).
2. Oliver, E. C. et al. Longer and more frequent marine heatwaves over the past century. *Nat. Commun.* **9**, 1324 (2018).
3. Giraldo-Ospina, G. et al. Marine heatwaves exacerbate climate change impacts for coastal ecosystems. *Sci. Rep.* **10**, 1–12 https://doi.org/10.1038/s41598-020-63650-z (2020).
4. Wyatt, A. S. J. et al. Hidden heatwaves and severe coral bleaching linked to mesoscale eddies and thermocline dynamics. *Nat. Commun.* **14**, 25 https://doi.org/10.1038/s41467-022-35550-5 (2023).
5. Piatt, J. F. et al. Extreme mortality and reproductive failure of common murres resulting from the northeast Pacific marine heatwave of 2014–2016. *PLoS ONE* **15**, e0226087 https://doi.org/10.1371/journal.pone.0226087 (2020).
6. Frölicher, T. L., Fischer, E. M. & Gruber, N. Marine heatwaves under global warming. *Nature* **560**, 360–364 https://doi.org/10.1038/s41586-018-0383-97 (2018).
7. Jacobs, Z. L. et al. Marine heatwaves and cold spells in the Northeast Atlantic: what should the UK be prepared for? *Front. Mar. Sci.* **11**, 1434365 https://doi.org/10.3389/fmars.2024.1434365 (2024).
8. Gou, R., Wolf, K. K. E., Hoppe, C. J. M., Wu, L. & Lohmann, G. The changing nature of future Arctic marine heatwaves and its potential impacts on the ecosystem. *Nat. Clim. Chang*. **15**, Article 2247 https://doi.org/10.1038/s41558-024-02224-7 (2025).
9. Tinker, J. et al. 21st century marine climate projections for the NW European Shelf Seas based on a Perturbed Parameter Ensemble. Preprint at https://doi.org/10.5194/egusphere-2023-1816 (2023).
10. Dong, T. et al. Record-breaking 2023 marine heatwaves. *Science* **389**, 369–375 https://doi.org/10.1126/science.adr0910 (2025).
11. Goreau, T. J. F. & Hayes, R. L. 2023 Record marine heat waves: coral reef bleaching HotSpot maps reveal global sea surface temperature extremes, coral mortality, and ocean circulation changes. *Oxf. Open Clim. Change* **4**, kgae005 https://doi.org/10.1093/oxfclm/kgae005 (2024).
12. England, M. H. et al. A record-breaking North Atlantic marine heatwave driven by atmospheric and oceanic variability. *Nature* **626**, 105–111 https://doi.org/10.1038/s41586-025-08903-5 (2025).
13. Guinaldo, T., Cassou, C., Sallée, J.-B. & Liné, A. Internal variability effect doped by climate change drove the 2023 marine heat extreme in the North Atlantic. *Commun. Earth Environ.* **6**, 291 https://doi.org/10.1038/s43247-025-02197-1 (2025).
14. Capotondi, A. et al. A global overview of marine heatwaves in a changing climate. *Commun. Earth Environ.* **5**, 297 (2024).
15. Huot, Y., Brown, C. A. & Cullen, J. J. Retrieval of phytoplankton biomass from simultaneous inversion of reflectance, the diffuse attenuation coefficient, and Sun-induced fluorescence in coastal waters. *J. Geophys. Res. Oceans* **112**, C06013 https://doi.org/10.1029/2006JC003794 (2007).
16. Roesler, C. et al. Recommendations for obtaining unbiased chlorophyll estimates from in situ chlorophyll fluorometers: a global analysis of WET Labs ECO sensors. *Limnol. Oceanogr. Methods* **15**, 572–585 https://doi.org/10.1002/lom3.10185 (2017).
17. Le Grix, N., Cheung, W. L., Reygondeau, G., Zscheischler, J. & Frölicher, T. L. Extreme and compound ocean events are key drivers of projected low pelagic fish biomass. *Glob. Change Biol.* **29**, 6478–6492 (2023).
18. Sharples, J. et al. Phytoplankton distribution and survival in the thermocline. *Limnol. Oceanogr.* **46**, 486–496 https://doi.org/10.4319/lo.2001.46.3.0486 (2001).
19. Chen, Z., Sun, J., Gu, T., Zhang, G. & Wei, Y. Nutrient ratios driven by vertical stratification regulate phytoplankton community structure in the oligotrophic western Pacific Ocean. *Ocean Sci.* **17**, 1775–1789 https://doi.org/10.5194/os-17-1775-2021 (2021).

20. Simpson, J. H. & Bowers, D. G. The role of tidal stirring in controlling the seasonal heat cycle in shelf seas. *Ann. Geophys.* **2**, 411–416 (1977).
21. Sharples, J. et al. Spring–neap modulation of internal tide mixing and vertical nitrate fluxes at a shelf edge in summer. *Limnol. Oceanogr.* **52**, 1735–1747 https://doi.org/10.4319/lo.2007.52.5.1735 (2007).
22. Bian, C., Jing, Z., Wang, H. & Wu, L. Scale-dependent drivers of marine heatwaves globally. *Geophys. Res. Lett.* **51**, e2023GL107306 https://doi.org/10.1029/2023GL107306 (2024).
23. Su, S., Fu, Y.-X., Sun, W. & Dong, J. Marine heatwaves and cold spells accompanied by mesoscale eddies globally. *Remote Sens* **17**, 2468 https://doi.org/10.3390/rs17142468 (2025).
24. Eppley, R. W. Temperature and phytoplankton growth in the sea. *Fish. Bull.* **70**, 1063–1085 (1972).
25. Brown, J. H., Gillooly, J. F., Allen, A. P., Savage, V. M. & West, G. B. Toward a metabolic theory of ecology. *Ecology* **85**, 1771–1789 https://doi.org/10.1890/03-9000 (2004).
26. Le Grix, N., Zscheischler, J., Laufkötter, C., Rousseaux, C. S. & Frölicher, T. L. Compound high-temperature and low-chlorophyll extremes in the ocean over the satellite period. *Biogeosciences* **18**, 2119–2137 (2021).
27. Le Grix, N., Zscheischler, J., Rodgers, K. B., Yamaguchi, R. & Frölicher, T. L. Hotspots and drivers of compound marine heatwaves and low net primary production extremes. *Biogeosciences* **19**, 5807–5835 (2022).
28. Noh, K. M., Lim, H.-G. & Kug, J.-S. Global chlorophyll responses to marine heatwaves in satellite ocean color. *Environ. Res. Lett.* **17**, 064034 https://doi.org/10.1088/1748-9326/ac70ec (2022).
29. Montie, S., Thomsen, M. S., Rack, W. & Broady, P. A. Extreme summer marine heatwaves increase chlorophyll *a* in the Southern Ocean. *Antarct. Sci.* **32**, 508–509 (2020).
30. Hayashida, H., Matear, R. J. & Strutton, P. G. Background nutrient concentration determines phytoplankton bloom response to marine heatwaves. *Glob. Change Biol.* **26**, 4800–4811 https://doi.org/10.1111/gcb.15255 (2020).
31. Williams, C., Sharples, J., Green, M., Mahaffey, C. & Rippeth, T. The maintenance of the subsurface chlorophyll maximum in the stratified western Irish Sea. *Limnol. Oceanogr.: Fluids Environ.* **3**, 61–73 https://doi.org/10.1215/21573689-2285100 (2013).
32. Williams, C., Sharples, J., Mahaffey, C. & Rippeth, T. Wind-driven nutrient pulses to the subsurface chlorophyll maximum in seasonally stratified shelf seas. *Geophys. Res. Lett.* **40**, 5467–5472 https://doi.org/10.1002/2013GL058171 (2013).
33. Tweddle, J. F., Sharples, J., Palmer, M. R., Davidson, K. & McNeill, S. Enhanced nutrient fluxes at the shelf sea seasonal thermocline caused by stratified flow over a bank. *Prog. Oceanogr.* **117**, 37–47 (2013).
34. Hickman, A. E. et al. Primary production and nitrate uptake within the seasonal thermocline of a stratified shelf sea. *Mar. Ecol. Prog. Ser.* **463**, 39–57 (2012).
35. Hobday, A. J. et al. Categorizing and naming marine heatwaves. *Prog. Oceanogr.* **161**, 227–238 https://doi.org/10.1016/j.pocean.2018.03.007 (2018).
36. Berthou, S. et al. Exceptional atmospheric conditions in June 2023 generated a northwest European marine heatwave which contributed to breaking land temperature records. *Commun. Earth Environ.* **5**, 1413 https://doi.org/10.1038/s43247-024-01413-8 (2024).
37. McCarthy, G. D. et al. Marine heatwave conditions around Ireland during June 2023. *Weather* **79**, 242–248 https://doi.org/10.1002/wea.4498 (2024).
38. Rippeth, T. R. Mixing in seasonally stratified shelf seas: a shifting paradigm. *Philos. Trans. R. Soc. A* **363**, 2837–2854 https://doi.org/10.1098/rsta.2005.1662 (2005).
39. Burchard, H. & Rippeth, T. P. Generation of bulk shear spikes in shallow stratified tidal seas. *J. Phys. Oceanogr.* **39**, 969–985 https://doi.org/10.1175/2008JPO4074.1 (2009).
40. Simpson, J. H., Tinker, J., Hunter, J. R. & Morris, N. C. G. The vertical structure of turbulent dissipation in shelf seas. *J. Phys. Oceanogr.* **26**, 1579–1590 (1996).
41. Rippeth,T. P. et al. The diapycnal nutrient flux and shear-induced diapycnal mixing in the seasonally stratified western Irish Sea. *Cont. Shelf Res.* **29**, 1580–1587 https://doi.org/10.1016/j.csr.2009.04.009 (2009).
42. Williams, C. A. J. et al. The Three Rs: Resolving Respiration Robotically in Shelf Seas. *Geophys. Res. Lett.* **49**, e2021GL096921 https://doi.org/10.1029/2021GL096921 (2022).
43. Masuda, Y. et al. Photoacclimation by phytoplankton determines the distribution of global subsurface chlorophyll maxima in the ocean. *Commun. Earth Environ.* **2**, 201 https://doi.org/10.1038/s43247-021-00201-y (2021).
44. Ma, X. & Chen, G. Marine heatwaves are shaping the vertical structure of phytoplankton in the global ocean. *Commun. Earth Environ*. **6**, Article 435 https://doi.org/10.1038/s43247-025-02718-y (2025).
45. Malan, N. et al. Lifting the lid on marine heatwaves. *Prog. Oceanogr.* **239**, 103539 https://doi.org/10.1016/j.pocean.2025.103539 (2025).
46. Schaeffer, A., Sen Gupta, A. & Roughan, M. Seasonal stratification and complex local dynamics control the sub-surface structure of marine heatwaves in Eastern Australian coastal waters. *Commun. Earth Environ.* **4**, 304 https://doi.org/10.1038/s43247-023-00966-4 (2023).
47. Arteaga, L. & Rousseaux, C. S. Marine heatwaves in the northeast Pacific amplify the biological impact of the Blob. *Commun. Biol.* **6**, 460 https://doi.org/10.1038/s42003-023-04645-0 (2023).
48. Sharples, J. et al. Internal tidal mixing as a control on continental margin ecosystems. *Geophys. Res. Lett.* **36**, L23603 https://doi.org/10.1029/2009GL040683 (2009).
49. Houde, E. D. Fish early life dynamics and recruitment variability. *Am. Fish. Soc. Symp.* **2**, 17–29 https://doi.org/10.47886/afs.2.17-29 (1987).
50. Cushing, D. H. Plankton production and year-class strength in fish populations: an update of the match/mismatch hypothesis. *Adv. Mar. Biol.* **26**, 249–293 https://doi.org/10.1016/S0065-2881(08)60202-3 (1990).
51. Cushing, D. H. *Population Production Regulation in the Sea: A Fisheries Perspective* (Cambridge University Press, 1995).
52. Embling, C. B., Sharples, J., Armstrong, E., Palmer, M. R. & Scott, B. E. Fish behaviour in response to tidal variability and internal waves over a shelf sea bank. *Prog. Oceanogr.* **117**, 106–117 https://doi.org/10.1016/j.pocean.2013.06.013 (2013).
53. Boyd, P. & Newton, P. Evidence of the potential influence of planktonic community structure on the interannual variability of particulate carbon flux. *Deep-Sea Res. Part I* **42**, 619–639 (1995).
54. Boyd, P. W. & Newton, P. Measuring biogenic carbon flux in the ocean. *Science* **275**, 554 (1997).
55. Legendre, L. & Rivkin, R. Fluxes of carbon in the upper ocean: regulation by food-web control nodes. *Mar. Ecol. Prog. Ser.* **242**, 95–109 https://doi.org/10.3354/meps242095 (2002).
56. Smith, K. E. et al. Baseline matters: challenges and implications of different marine heatwave baselines. *Prog. Oceanogr.* **231**, 103404 https://doi.org/10.1016/j.pocean.2024.103404 (2025).
57. Jackson, T., Calton, B. & Hockley, K. *C3S Ocean Colour Version 6.0: Product User Guide and Specification* (Copernicus Climate Change Service, 2023).
58. Garau, B. et al. Thermal lag correction on Slocum CTD glider data. *J. Atmos. Ocean. Technol.* **28**, 1065–1071 https://doi.org/10.1175/JTECH-D-10-05030.1 (2011).
59. Thomalla, S. J. et al. An optimized method for correcting fluorescence quenching using optical backscattering on autonomous platforms.

Limnol. Oceanogr. Methods **16**, 132–144 https://doi.org/10.1002/lom3.10234 (2018).
60. de Boyer Montégut, C. et al. Mixed layer depth over the global ocean: an examination of profile data and a profile-based climatology. *J. Geophys. Res. Oceans* **109**, C12003 https://doi.org/10.1029/2004JC002378 (2004).

Acknowledgements

We thank Steve Woodward and Alexander Cerra from Marine Autonomous Robotic Systems (MARS) at the National Oceanography Centre for their assistance with deploying, piloting and recovering the glider. We also thank the Marine Directorate of the Scottish Government for conducting the chlorophyll sampling and analysis and ADCP recovery, and the officers and crews of the RV Corystes (Agri-Food and Biosciences Institute, Belfast) for their assistance in collecting the observations.

Author contributions

C.A.J.W. carried out glider processing, data analysis and wrote the manuscript. J.E.H. made a major contribution to the analysis and interpretation of the glider data. M.R.P., J.U.W. and T.P.R. contributed to the interpretation of the physical oceanographic observations and results. Z.J. contributed to the chlorophyll climatology analysis. R.O.M. led the CTD, water sample collection and analysis. B.E.S. led the project and contributed to the interpretation of the ecological implications of chlorophyll variability for higher trophic levels.

Funding

This research was conducted as part of the Physics to Ecosystem Level Assessment of Impacts of Offshore Windfarms (PELAgIO) project, which forms part of the Ecological Consequences of Offshore Wind (ECOWind) programme. ECOWind is co-funded by the Natural Environment Research Council (NERC) and the Offshore Wind Evidence and Change (OWEC) Programme under grant NE/X008835/1 (B.E.S.). J.E.H. was supported by NERC grant NE/Y005589/1.

Competing interests

The authors declare no competing interests.

Additional information

Supplementary information The online version contains supplementary material available at https://doi.org/10.1038/s43247-026-04118-2.

Correspondence and requests for materials should be addressed to Charlotte A. J. Williams.

Peer review information *Communications Earth & Environment* thanks all reviewer(s) for their contribution to the peer review of this work. Primary Handling Editors: Weiqing Han and Alice Drinkwater. A peer review file is available.

Reprints and permissions information is available at http://www.nature.com/reprints

Publisher's note Springer Nature remains neutral with regard to jurisdictional claims in published maps and institutional affiliations.

Open Access This article is licensed under a Creative Commons Attribution 4.0 International License, which permits use, sharing, adaptation, distribution and reproduction in any medium or format, as long as you give appropriate credit to the original author(s) and the source, provide a link to the Creative Commons licence, and indicate if changes were made. The images or other third party material in this article are included in the article's Creative Commons licence, unless indicated otherwise in a credit line to the material. If material is not included in the article's Creative Commons licence and your intended use is not permitted by statutory regulation or exceeds the permitted use, you will need to obtain permission directly from the copyright holder. To view a copy of this licence, visit http://creativecommons.org/licenses/by/4.0/.

© The Author(s) 2026

This Article in Press is shared early to give you faster access to new research. It is citable and carries a permanent DOI. The final edited version will replace it automatically.